JOURNAL OF AIRCRAFT
Vol. 48, No. 4, July–August 2011

Boundary-Layer Suction System Design for Laminar-Flying-Wing Aircraft

T. I. Saeed,* W. R. Graham,† and C. A. Hall‡
University of Cambridge, Cambridge, England CB2 1PZ, United Kingdom

DOI: 10.2514/1.C031283

The present study aims to provide insight into the parameters affecting practical laminar-flow-control suction power requirements for a commercial laminar-flying-wing transport aircraft. It is shown that there is a minimum power requirement independent of the suction system design, associated with the stagnation pressure loss in the boundary layer. This requirement increases with aerofoil section thickness, but depends only weakly on Mach number and (for a thick, lightly loaded laminar flying wing) lift coefficient. Deviation from the optimal suction distribution, due to a practical chamber-based architecture, is found to have very little effect on the overall suction coefficient; hence, to a good approximation, the power penalty is given by the product of the optimal suction flow rate coefficient and the average skin pressure drop. In the spanwise direction, through suitable choice of chamber depth, the pressure drop due to frictional and inertial effects may be rendered negligible. Finally, if there are fewer pumps than chambers, the average pressure drop from the aerofoil surface to the pump collector ducts, rather than to the chambers, determines the power penalty. For the representative laminar-flying-wing aircraft parameters considered here, the minimum power associated with boundary-layer losses alone contributes some 80–90% of the total power requirement.

Nomenclature

A_R	=	wing aspect ratio
b	=	wingspan
c	=	chord length
c_p	=	specific heat capacity of air at constant pressure
C_l	=	section lift-coefficient
C_p	=	$\frac{P_e - P_\infty}{\frac{1}{2}\rho_\infty U_\infty^2}$, surface pressure coefficient
C_f	=	wall skin-friction coefficient
C_d	=	dissipation coefficient
C_Q	=	$\oint \frac{V_0}{U_\infty}\,\mathrm{d}(s/c)$, suction flow coefficient
d	=	suction hole diameter
D^*	=	dissipation function for a laminar boundary layer
D_{eq}	=	$2h\frac{w_c/h}{1+w_c/h}$, equivalent diameter for rectangular conduits
f	=	friction factor
h	=	chamber height
H_{12}	=	δ_1/δ_2, shape factor
H_{32}	=	δ_3/δ_2, energy shape factor
k	=	$\tilde{P}_\infty - \tilde{P}_c$, nondimensional pressure difference constant
K_s	=	skin resistance
$\dot{m}$	=	mass flow rate per unit width along spanwise chamber
$\dot{m}_s$	=	area-distributed suction mass flow rate
M_∞	=	freestream Mach number
P, $\tilde{P}$	=	pressure; $\frac{P}{\frac{1}{2}\rho_\infty U_\infty^2}$, nondimensional pressure
$\tilde{r}_c$	=	$\frac{\Delta\tilde{P}_{s,\max}}{\Delta\tilde{P}_{s,\min}}$, ratio of nondimensional pressure difference across skin over a single chamber width
Re_c	=	$U_\infty c/\nu$, chord Reynolds number
$Re_{D_{\mathrm{eq}}}$	=	$\frac{2\dot{m}}{\mu}\frac{w_c/h}{1+w_c/h}$, spanwise-chamber Reynolds number
Re_h	=	$V_h d/\nu$, suction hole Reynolds number
Re_{δ_2}	=	$u_e\delta_2/\nu$, momentum Reynolds number
s	=	intrinsic distance along aerofoil
t	=	maximum section thickness
t_s	=	skin thickness
T	=	temperature
u_e	=	local velocity outside boundary layer
U_∞	=	freestream velocity
V_0	=	area-distributed suction velocity
V_h	=	hole suction velocity
W	=	aircraft cruise weight
w_c	=	chamber width
$\tilde{w}_p$, $\tilde{W}_p$	=	area-distributed, and total, power coefficient
x	=	chordwise distance
z, $\tilde{z}$	=	spanwise distance, z/b, nondimensional spanwise distance
δ_1, δ_2, δ_3	=	boundary-layer displacement, momentum and kinetic energy thickness
ϵ^*	=	skin-friction function for a laminar boundary layer
ν	=	kinematic viscosity
ρ	=	density
ΔP, $\Delta\tilde{P}$	=	pressure difference; $\frac{\Delta P}{\frac{1}{2}\rho_\infty U_\infty^2}$, nondimensional pressure difference

Subscripts

∞	=	freestream
e	=	boundary-layer edge
0	=	stagnation quantity
w	=	wall
h	=	hole
s	=	skin
c	=	chamber
d	=	duct
in	=	pump inlet
ex	=	pump exit

Superscripts

$'$	=	first-order differentiation with respect to s

Presented at the 28th Applied Aerodynamics Conference, Chicago, IL, 28 June–1 July 2010; received 27 October 2010; revision received 10 January 2011; accepted for publication 21 February 2011.

*Research Student in Fluid Mechanics, Department of Engineering. Student Member AIAA.
†Senior Lecturer in Aircraft Aerodynamics, Department of Engineering. Member AIAA.
‡University Lecturer, Department of Engineering. Member AIAA.

I. Introduction

WITH the growing traffic in air travel, focus is being increasingly drawn to the environmental impact caused by commercial aircraft emitting combustion products into the high-level atmosphere. Whilst new aircraft continue to achieve some reductions in fuel-burn and harmful emissions, the possible improvements are constrained by the overall configuration, which to a large extent has not changed in the last 50 years. In contrast, the Greener by Design group has suggested that a 70% reduction in fuel-burn per passenger could be achieved by an LFW (laminar-flying-wing) aircraft having 2050 technology, relative to current aircraft of 2001 technology [1].

The LFW uses distributed suction as a means of LFC (laminar flow control) through porous wing surfaces; the effect of suction on the flow is two-fold: first, there is a reduction in local Reynolds number with the thinning of the boundary layer; and second, the vorticity distribution within the boundary layer is altered so that a more stable flow is established [2]. The aim of using LFC is to maintain a laminar boundary layer at a Reynolds number where it would typically be turbulent, and thereby reduce drag.

The LFW layout lends itself well to LFC as there is a much higher percentage of wetted area that can be laminarized in comparison with conventional aircraft designs, where the fuselage poses a problem [3]. However, drag reduction using LFC requires power to energize the suction system, which must discharge the sucked boundary-layer flow at freestream pressure and a desired velocity. This additional power requirement is a key parameter influencing the overall performance of the aircraft.

Previous studies of the required power have mainly focussed on trying to minimize the suction system losses. In summarizing research conducted at Northrop, Pfenninger [4] considers throttling and mixing losses, flow separation, duct-wall friction, and secondary-flow losses, and proposes a number of novel solutions to minimize them. However, compared with the losses associated with the deceleration of the flow in the boundary layer, the additional contributions through the suction system seem fairly small. Lachmann [5] and Gregory [6] have both stated that the main effort should be in overcoming boundary-layer losses. Gregory [6] also noted that low additional suction power demands a porous surface whose resistance to flow varies over the chord, to minimize unwanted variations; Head [7] and Lachmann [5] incorporated such a resistance into throttle holes situated in a cellular subsurface structure. A final strategy for minimizing the additional power is suggested by Pearce [8]: in regions where the suction requirements are high, triangular chambers of full aerofoil section depth may be implemented to minimize losses in transporting the flow along the wing to the suction pumps.

As a result of these studies, the basic architecture of a practical LFC suction system is well established. However, there is still little general guidance available on the important design parameters and their interactions. Furthermore, the requirements imposed on the system by a passenger-carrying LFW are likely to differ significantly from the conventional context [9]. To attain the full benefit from the viscous drag reduction, the induced drag must also be small, which in turn requires a wing with low span loading, $(W/b)^2$, operating at a lift coefficient below conventional values. (The latter requirement is under the control of the designer, as a larger span will allow higher values; however, this shifts the design towards extreme aspect ratios.) The large-span constraint then leads to a low sweepback design (for structural reasons) and, in conjunction with a fixed minimum for the cabin height, thick aerofoil sections. Finally, the freedom to optimize section geometry will be severely restricted by passenger accommodation and moment balance requirements. These changes will reduce the applicability of the past studies to the configuration of interest here.

The aim of the present study is thus to provide insight into the parameters affecting practical LFC suction power requirements for a commercial LFW transport aircraft. Specifically, our objectives are: to characterize the increased power requirement due to the individual system elements, relative to the theoretical minimum associated with the unavoidable boundary-layer losses; to investigate the tradeoff between reduction of the additional power requirement and increasing system complexity; and to formulate approximate calculation methods that may be of use in overall LFW design and optimization. The paper begins by introducing a boundary-layer stability code, which calculates the "optimal" distribution of suction for the maintenance of laminar flow; the influences of a number of key design parameters on the level of suction are then investigated; finally, the main contributors to the various pressure drops through the suction system are discussed in turn.

II. Boundary-Layer Suction Calculation Method

In developing a suction system design, the required level and distribution of suction for the maintenance of laminar flow must first be determined. In this section a boundary-layer solver is implemented and validated, and a suction algorithm is developed and compared against an example calculation by Head [10].

A. Boundary-Layer Solver

The current industry standard for transition prediction is the e^N-method, which is based on the growth rate of linear instabilities in the boundary-layer flow and empirically determined criteria for the degree of growth necessary for transition to occur [11]. In general, there are several classes of instability that cause transition. However, as the high-aspect-ratio LFW demands low wing-sweep, we assume that attention can be restricted to the influence of two-dimensional Tollmien–Schlichting instabilities. (This limits our analysis to sweep angles below about 25° [11].) In this case simpler methods, which are more computationally efficient, may be employed; here we use Eppler and Somers' [12] two-dimensional semi-empirical computational model, which has been shown to give excellent predictions of transition in wind-tunnel experiments [13].

The computational analysis is divided into inviscid and viscous steps. The aerofoil surface is discretized into a number of panels. The inviscid calculation is performed using "Xfoil" [14], which calculates the aerofoil surface-pressure distribution via an incompressible vortex-panel method combined with a compressibility correction. (The default number of panels in Xfoil is 160, with a maximum of 354. The accuracy in the final calculated suction quantity was found to worsen with increases in maximum section thickness and freestream Mach number; C_l variation had no effect. For a NACA0030 aerofoil, with $M_\infty = 0.5$ and $C_l = 0$, there is an error of 1.3% between the default and maximum number of panels.) The viscous analysis takes the pressure distribution and, for a specified chord Reynolds number, calculates the development of the boundary layer using the Eppler and Somers [12] method.

Eppler and Somers' method [12] is based on a numerical solution of the (incompressible) integral momentum and energy equations:

$$\delta_2' + (2 + H_{12})\frac{u_e'}{u_e}\delta_2 = C_f - \frac{V_0}{u_e} \tag{1}$$

and

$$\delta_3' + 3\frac{u_e'}{u_e}\delta_3 = C_d - \frac{V_0}{u_e} \tag{2}$$

respectively, where: $C_f = \epsilon^*/Re_c \frac{u_e}{U_\infty}\frac{\delta_2}{c}$; $C_d = 2D^*/Re_c \frac{u_e}{U_\infty}\frac{\delta_2}{c}$; and ϵ^*, D^*, H_{12} are functions of the energy shape factor H_{32}.

The location of transition is based on a critical momentum thickness, which is a function of H_{32} only:

$$\ell_n(Re_{\delta_2}) = 18.4H_{32} - 21.78 \tag{3}$$

Previous boundary-layer stability studies, using the e^N-method, have found that, in the case of excessive suction, the critical amplification value N for the onset of transition reduces, i.e., the transition criteria for sucked and unsucked flows are not identical [15]. Eppler [16] comments that, because suction is normally combined with finite disturbances, transition mostly occurs before the linear stability limit is reached. For $H_{32} > 1.62$, which can only be reached by suction,

Eppler and Somers' [12] empirical criterion predicts transition well before that corresponding to the linear stability limit.

At low local Mach numbers, the influence of compressibility on the stability of the boundary layer may be taken as negligible; in fact, the well-established Orr–Somerfield equation has this as an underlying assumption [17]. For subcritical flow regimes, compressibility effects become increasingly important with Mach number, with the growth rate of the Tollmien–Schlichting type instability reducing as a consequence. This highly stabilizing influence was exploited by Viken and Wagner [18] in the design of high-speed natural-laminar-flow aerofoils. Mack [19], through a linear stability analysis, found that incompressible codes overpredict the local amplification rates. Harris et al. [20] performed experimental investigations on a swept-supercritical aerofoil employing LFC and calculated that, relative to incompressible predictions, compressibility effects reduced the amplification values in the midchord Tollmien–Schlichting wave dominated regions by approximately 40%. Harris et al. [20] chose to base their final suction system design on the incompressible calculations, due to the increased conservatism of the estimated suction requirements that follow. Further studies on the influence of compressibility can be found in the works of Atkin [21], Bushnell and Malik [22], and Berry et al. [23]. However, the literature does not provide a quantitative indication of the likely error in incompressible LFC suction calculations.

Nonetheless, the simplicity and conservatism of an approach employing the incompressible form of the integral equations make it attractive. Furthermore, surface roughness effects [11] are neglected in the present study, and a conservative calculation goes some way in compensating for this. Subsequently, therefore, only the influence of Mach number on the surface pressure distribution is accounted for. The integral boundary-layer equations are solved using a standard fourth-order Runge–Kutta algorithm with adaptive spacing, with the relative error tolerance set to 0.1%.

The laminar-boundary-layer solver was first validated by modelling a zero-pressure-gradient flow over a flat plate: the δ_2 variation was in agreement with Blasius's prediction [24]. Next, assuming a linearly retarded velocity profile, the code's ability to predict laminar separation was confirmed against Howarth's boundary-layer calculation [24]. Further checks, for pressure distributions corresponding to a range of symmetric aerofoil thicknesses, lift coefficients and chord-based Reynolds numbers, were made against Thwaites' method [24] with excellent results.

Over certain regions of the aerofoil, suction may not be permissible. Therefore it is also necessary to solve Eqs. (1) and (2) for a turbulent boundary-layer. The only differences that arise are the forms of C_f, C_d, and the empirical relations depending on H_{32}. Turbulent separation is flagged when H_{32} drops below 1.46.

B. Suction Algorithm and Validation

A calculation method is required such that the power demanded to maintain laminar flow is kept to a minimum. Head [10] claimed that applying just enough suction to keep the boundary layer in a condition of neutral stability would give a total power requirement which approximates closely to that minimum. While not immediately evident, this claim can be supported by a simple argument. On consideration of the minimum (incompressible) pump- power per unit span required to return the sucked flow to the freestream stagnation pressure:

$$\int_0^c [P_{0,\infty} - P_w] V_0 \, \mathrm{d}x$$

and assuming, as an approximation, that suction is only necessary in regions of adverse pressure gradient, it is apparent that suction earlier, where P_w is lower, is penalized more than suction later on. Therefore, in determining V_0 we aim always to choose the minimum allowable value, i.e., to maintain the boundary layer on the verge of transition. This can be achieved via the following algorithm.

Consider the integral momentum and energy Eqs. (1) and (2): assuming C_f and C_d are not significantly affected by the application of surface suction, the energy shape factor at the end of a panel of length Δs may be estimated as:

$$H_{32} = \frac{\delta_3^{(i+1)} - (V_0/u_e)\Delta s}{\delta_2^{(i+1)} - (V_0/u_e)\Delta s} \tag{4}$$

where $i+1$ denotes the conditions at the end of the panel which would apply in the absence of suction. To maintain the boundary layer on the verge of transition, V_0 should be set such that the stability criterion given by Eq. (3) is not flagged; a target energy shape factor $H_{32}^{(t)}$ is thereby defined and set equal to the right-hand side of Eq. (4). On rearrangement, we obtain an initial estimate of the suction velocity required:

$$\frac{V_0}{u_e} = \frac{(H_{32}^{(t)} - H_{32}^{(i+1)})\delta_2^{(i+1)}}{(H_{32}^{(t)} - 1)\Delta s} \tag{5}$$

The initial suction estimate may deviate significantly from the minimum required, especially in regions where C_p changes considerably. Therefore, the calculation is then iterated to find the optimized panel suction corresponding to Head's [10] criterion.

To assess the accuracy of the algorithm, the distribution of suction calculated for a NACA $65_4 - 021$ aerofoil at zero incidence (with an incompressible surface velocity distribution as shown in Fig. 1) and for an Re_c of 20 million, is compared against Head's prediction [10] in Fig. 2. NACA 6-series aerofoils were designed to maintain natural laminar flow over a large percentage of chord by delaying the adverse pressure gradient. The thickness envelope was developed using aerofoil theory; however, no simple definition of the shape is available [25]. The aerofoil required here was generated using Ladson and Brooks' [25] computational program, which provides a reasonable approximation to the thickness distribution. The corresponding velocity distribution was then generated using Xfoil [14]. It agrees closely with that given by Head [10] (also shown in Fig. 1).

The calculated level of distributed suction compares very well with Head's prediction [10] downstream of 40% chord. The obvious difference between the two distributions is the chordwise position at which suction is initiated; this is due to the difference between Lin's transition criterion (which Head uses in conjunction with the Thwaites solution for a laminar boundary-layer) and Eppler and Somers'[12]. Both predict transition within the weakly favorable pressure-gradient region between 10 and 45% chord (as might be expected for such a high Reynolds number), but Lin's does so earlier. Head [10] estimates (for the upper and lower surface combined) $C_Q = 5.14 \times 10^{-4}$; here, it is calculated that $C_Q = 5.18 \times 10^{-4}$, the discrepancy, in terms of volumetric flow rate, is negligible.

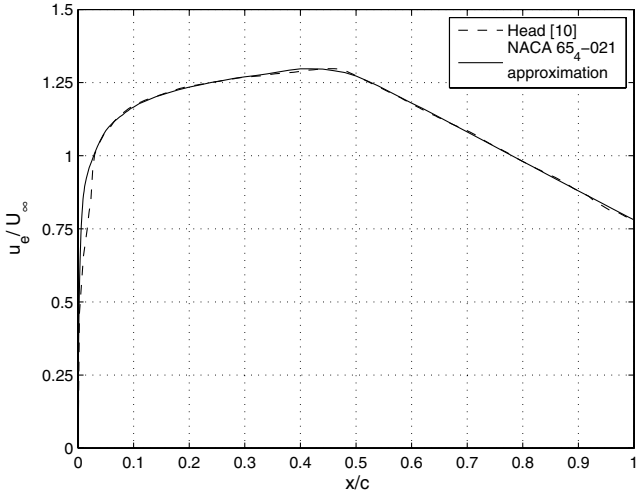

Fig. 1 NACA $65_4 - 021$ incompressible surface velocity distribution: $C_l = 0$.

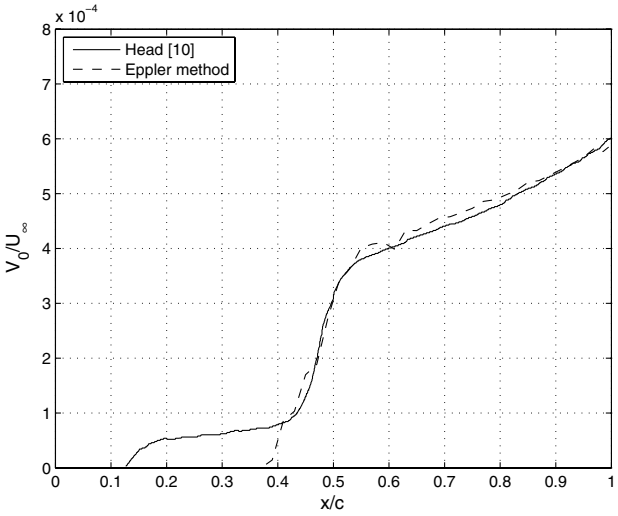

Fig. 2 Comparison of calculated suction distribution: NACA $65_4 - 021$ aerofoil, $C_l = 0$ and $Re_c = 20 \times 10^6$.

A final comparison is made against Head's [10] calculated momentum thickness distribution in Fig. 3. There is excellent agreement between the two methods.

III. Pump Power Analysis

With the method of calculating the desired pattern of inflow to maintain laminar flow determined, it remains to estimate the power input necessary to drive the suction system. In this section, a nondimensional power coefficient is defined.

In addition to the stagnation pressure loss in the boundary layer, there is an associated drop across each of the hardware components (discussed later in Sec. V). The suction pumps are required to raise the stagnation pressure of the sucked flow back to a value that allows it to be discharged with some speed V at freestream static pressure. Assuming adiabatic and reversible flow across the pump, an area-distributed pump power coefficient $\tilde{w}_p$ is:

$$\tilde{w}_p = \frac{\rho V_0(x,z) c_p T_{0,\text{in}} (\text{PPR}^{\frac{\gamma-1}{\gamma}} - 1)}{\frac{1}{2}\rho_\infty U_\infty^2 . U_\infty} \tag{6}$$

where the pump pressure ratio $\text{PPR} = P_{0,\text{ex}}/P_{0,\text{in}}(x,z)$. The total pump power coefficient $\tilde{W}_p$ is subsequently:

$$\tilde{W}_p = \frac{1}{bc}\int_0^b \int_0^c \tilde{w}_p \, \mathrm{d}x \, \mathrm{d}z \tag{7}$$

The principal variables affecting these dimensionless coefficients are the distribution of suction flow rate V_0 and the increase in total pressure required across the pumps. The latter depends not only on the wing pressure distribution, porous skin, and ducting network, but also on the discharge velocity of the sucked flow.

The works by Head [7], Rioual et al. [26], and Edwards [27] have shown that, based on a consideration of the total power required to overcome drag forces, it is optimal to discharge at a velocity slightly above freestream velocity, depending on the relative efficiencies of the suction pump and aircraft propulsion systems. However, the benefit of the excess is typically small. Furthermore, Atkin [21] comments that the effect of losses in the system is to flatten the minimum in the pump-drag versus exhaust Mach number relationship. Finally, given that the engine sizing for an LFW aircraft is likely to be determined by takeoff requirements [9], increasing the discharge velocity above freestream could increase suction-pump weights without reducing propulsion system weight; therefore, a freestream exit velocity is unlikely to be far from optimal. In the absence of propulsion system information, we assume $V = U_\infty$ and hence $P_{0,\text{ex}} = P_{0,\infty}$.

IV. Minimum Suction Requirements

Once the wing geometry and flight condition are set, the minimum suction and power requirements can be determined independently of any details of the LFC suction system design. The aim of this section is to provide estimates of these requirements for the range of design parameters expected of an LFW aircraft, and to understand which parameters have the greatest influence.

First, recall the fundamental features identified as necessary by Saeed et al. [9]: a high aspect ratio and low C_l. When combined with a section height sufficient for passenger accommodation and structural considerations, this gives rise to a thick wing with low sweep. To keep the flow subcritical this requires a low cruise Mach number. Typical design parameter values are: $Re_c = 40 \times 10^6$, $t/c = 28\%$, $C_l = 0.15$ and $M_\infty = 0.56$. As the section geometry will be significantly constrained by nonaerodynamic considerations, NACA00 series aerofoils are selected for this study. We first characterize the suction requirements for the parameter values given above, and then investigate the variation with C_l, Re_c, M_∞, and maximum t/c.

A. Typical Suction and Power Distributions

The upper-surface C_p distribution for a NACA0028 aerofoil at the chosen design point is plotted in Fig. 4, along with the optimized distribution of suction required for laminarization. The suction

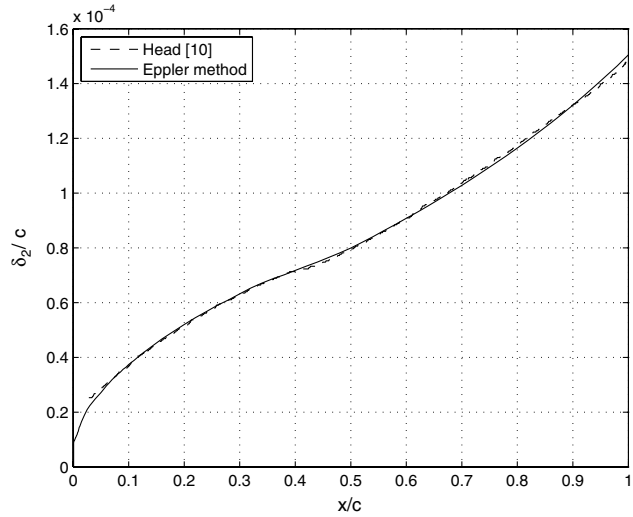

Fig. 3 Comparison of calculated momentum thickness distribution: NACA $65_4 - 021$ aerofoil, $C_l = 0$ and $Re_c = 20 \times 10^6$.

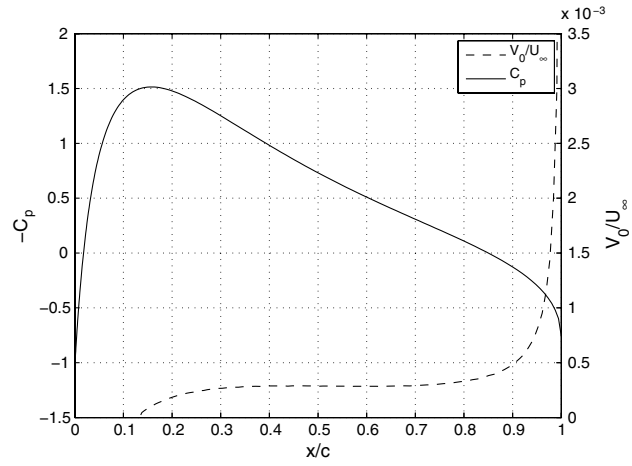

Fig. 4 Section pressure (solid) and suction velocity distribution (dashed) for the upper surface of a NACA0028 aerofoil: $M_\infty = 0.56$, $Re_c = 40 \times 10^6$, and $C_l = 0.15$.

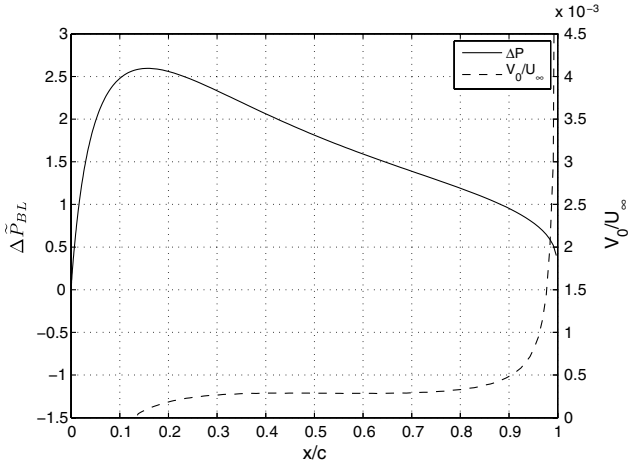

Fig. 5 Distribution of dynamic pressure loss through boundary layer (solid), and suction velocity (dashed) for the upper surface of a NACA0028 aerofoil: $M_\infty = 0.56$, $Re_c = 40 \times 10^6$, and $C_l = 0.15$.

requirement starts just upstream of the suction peak and remains reasonably constant until the severe adverse pressure gradient region over the last 10% of chord. The suction coefficient for the upper surface is $C_Q = 3.78 \times 10^{-4}$.

The loss in stagnation pressure associated with the boundary-layer flow is given by $\Delta P_{\mathrm{BL}} = P_{0,\infty} - P_e$ (based on Prandtl's assumption that the pressure across the boundary layer is constant [24]), and is plotted in dimensionless form in Fig. 5, which also repeats the suction velocity distribution. The (chordwise-distributed) minimum power requirement is approximately the product of these two quantities. However, for the exact minimum power calculation, we use Eqs. (6) and (7). Here $P_{0,\mathrm{in}} = P_e$, $P_{0,\mathrm{ex}} = P_{0,\infty}$ and, assuming adiabatic flow in the boundary layer, $T_{0,\mathrm{in}} = T_{0,\infty}$.

As discussed in Sec. II, the greatest stagnation pressure loss in the boundary layer is concentrated in regions of low pressure (for example, near the suction peak); consequently, although the sucked velocity is low in comparison with that toward the trailing edge, it is penalized heavily: this is evident from the distribution of $\tilde{w}_p$ in Fig. 6. The total pump power coefficient for the upper surface is $\tilde{W}_p = 4.11 \times 10^{-4}$. At the other extreme from this idealized minimum, one could envisage a suction system in which all the sucked flow entered a single chamber, with the pressure maintained just below the value of P_e at the suction peak, and with the suction velocity distribution achieved by varying the skin resistance. This is the basis of Pearce's [8] estimate of the power requirement; for this case it yields $\tilde{W}_p = 11.0 \times 10^{-4}$, almost three times greater than the minimum.

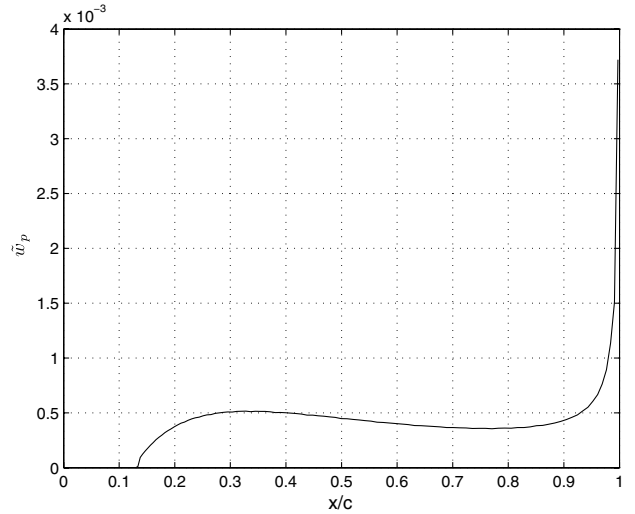

Fig. 6 Distribution of (area-distributed) power to overcome losses through boundary layer.

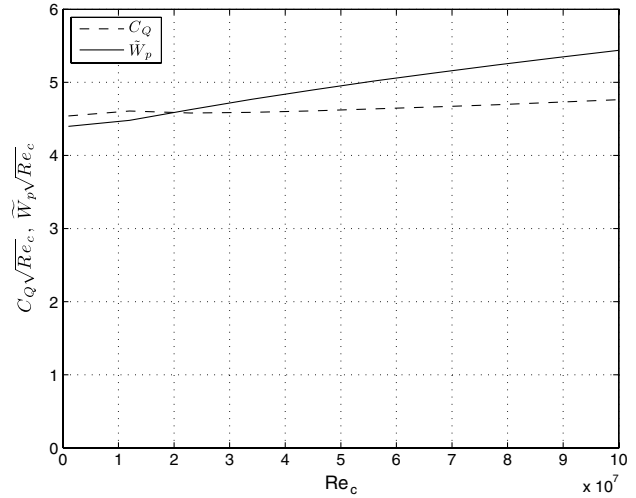

Fig. 7 Variation of C_Q and $\tilde{W}_p$ with Re_c: NACA0028, $C_l = 0.15$ and $M_\infty = 0.56$. Note that both variables are scaled by $\sqrt{Re_c}$, so that a constant level implies proportionality to $Re_c^{-1/2}$.

B. Parameter Study

The dependence of the overall suction coefficient (upper and lower surface combined) on chord Reynolds number is well established [28] as $C_Q \propto Re_c^{-1/2}$; this result is reproduced in Fig. 7 using the suction algorithm developed for the present study. From Eq. (6), we know that the power requirement depends directly on the distribution of V_0 and the pressure drop. The integrated area of $V_0\sqrt{Re_c}$ along the chord, i.e., $C_Q\sqrt{Re_c}$ is almost exactly independent of Re_c, as expected. However, as chord Reynolds number is increased, the suction initiation point moves further upstream, and the mean level of $V_0\sqrt{Re_c}$ over the suction region drops. Sucked flow near the surface pressure minimum is penalized more in terms of power, so this redistribution leads to the gradual increase in $\tilde{W}_p\sqrt{Re_c}$ with Re_c observed in Fig. 7.

The influence of t/c on suction is detailed in Fig. 8, for three NACA00 series aerofoils with maximum thickness-to-chord ratios of 10, 20, and 30%; the corresponding C_p distributions are also shown, using x markers. (A freestream Mach number of 0.5 is assumed here, otherwise the flow becomes supercritical for the highest value of t/c.) Increasing t/c delays transition, however, the overall suction magnitude increases as a result of the associated rise in adverse pressure gradient over the rear of the aerofoil.

For the range of C_l and t/c relevant to the LFW aircraft, Fig. 9a shows that t/c has a much greater effect on the overall suction

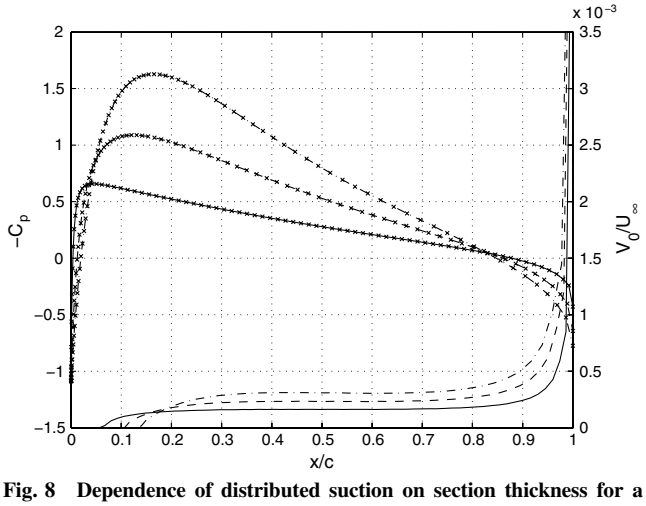

Fig. 8 Dependence of distributed suction on section thickness for a range of NACA00xx aerofoils at $C_l = 0.15$, $M_\infty = 0.5$, and $Re_c = 40 \times 10^6$: solid line: 10%; dashed line: 20%; and dashed-dotted line: 30%; x markers detail C_p.

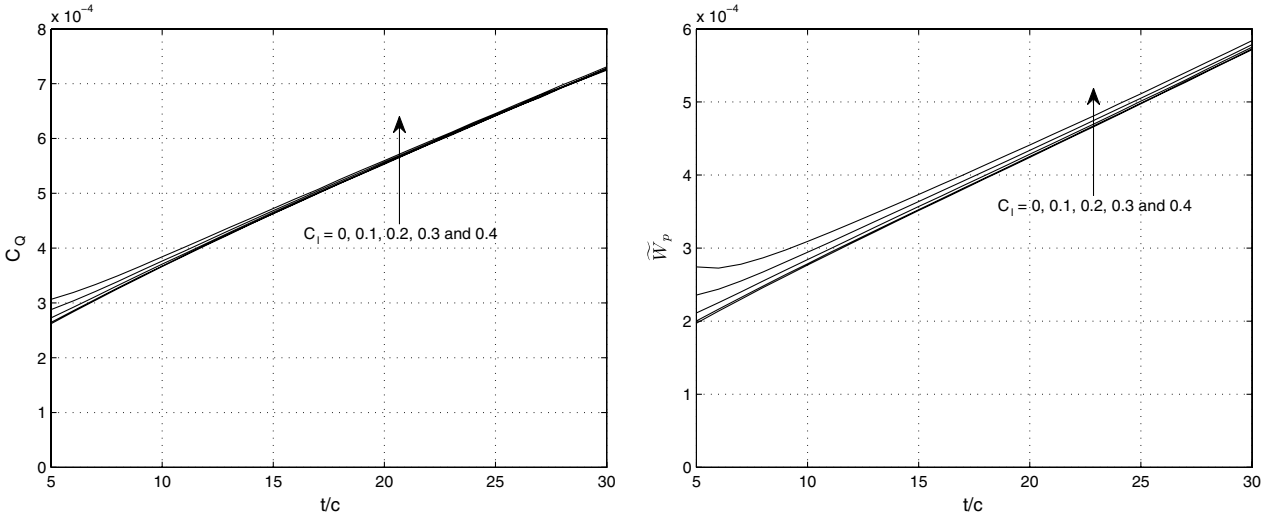

Fig. 9 Variation of a) C_Q and b) $\tilde{W}_p$ with maximum thickness-to-chord ratio and section lift coefficient: NACA00 series, $M_\infty = 0.5$ and $Re_c = 40 \times 10^6$.

requirement than C_l; the influence of the latter only becomes evident as t/c is reduced below 15%. The effect on $\tilde{W}_p$ is slightly stronger, as detailed in Fig. 9b. However, for the high thickness-to-chord ratios of interest in this study, the influence of C_l on the overall suction requirement is likely to be negligible; consequently, variations in C_l along the span of a properly designed LFW aircraft could possibly be neglected in initial calculations.

The influence of freestream Mach number and maximum section t/c on C_Q and $\tilde{W}_p$ is detailed in Fig. 10. Each line of constant t/c is plotted up to the Mach number at which the flow over the aerofoil first reaches the critical limit. At the lower Mach numbers, we do not expect the C_p distribution for a given C_l to vary significantly; hence the initial weak dependence of C_Q and $\tilde{W}_p$ on M_∞ for a fixed t/c is relatively unsurprising. As t/c and M_∞ increase, the effect of M_∞ becomes more noticeable, but not to the extent that it can be regarded as a significant influence.

V. Suction Hardware Design and Power Consumption

The power requirements associated with the inevitable loss in stagnation pressure through the boundary layer have been explored thus far. It now remains to specify a system to implement the LFC in practice. In this section a practical internal layout is proposed, consisting of spanwise chambers and chordwise ducts. The additional power demands associated with pressure drops across the porous skin, chambers and ducts are introduced in turn.

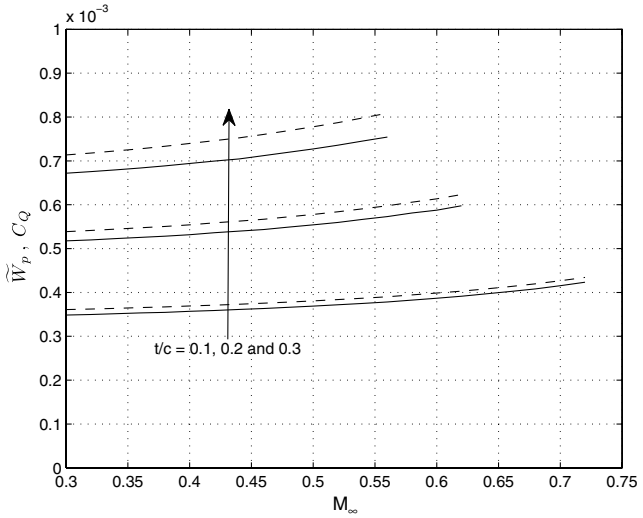

Fig. 10 Variation of C_Q (solid line) and $\tilde{W}_p$ (dashed line) with freestream Mach number and maximum thickness-to-chord ratio: NACA00 series, $C_l = 0.15$ and $Re_c = 40 \times 10^6$.

The typical LFW design parameter values and wing section geometry, specified in Sec. IV, are used. However, at this point, for clarity, we restrict consideration to the upper surface of the wing only. We also neglect spanwise variations in chord.

A. Suction Chamber Layout

One possible internal pipework arrangement is a single collector duct receiving sucked air from all over the wing. However, pressure recovery over the rear of the aerofoil means that the driving pressure across the skin will increase significantly, making it difficult to attain the desired suction distribution with a constant skin resistance. Gregory [6] (and others such as Lachmann [5]) proposed that the ideal solution would be to have a number of pumps, or several stages in one pump, so that the applied pressure difference can be varied over the surface of the wing, thus keeping the flow rates across the skin to a minimum; or, alternatively, to grade the skin resistance. The latter approach, however, is a less efficient solution; although the correct flow rates are maintained, the pressure difference between the surface and pump entry will be greater than necessary in the high resistance regions.

A plan view of the proposed suction hardware configuration is illustrated in Fig. 11: the LFW aircraft would consist of several such arrangements along its span. The boundary-layer fluid is sucked through the porous skin and then transported along spanwise chambers to a set of chordwise collector ducts; each duct feeds a pump, which ejects the sucked fluid into the freestream. Spanwise chambers, instead of chordwise, are adopted because they are structurally more efficient, allowing for integration with the main wing box stiffeners [8]; furthermore, this arrangement minimizes variations in the difference between the outer surface pressure and the (almost-constant) chamber pressure. Finally, given the space constraints imposed by a sharp-trailing-edge aerofoil, laminarization is assumed possible up to 90% chord only.

B. Skin Losses and Chamber Discretization

The chamber layout shown will provide a piecewise-constant subsurface pressure distribution. In this section, an algorithm is developed to specify this distribution, along with a skin-resistance gradation, and then calculate the resulting "real" suction flow. First, the analytical expression that relates the suction velocity across the porous skin to the applied pressure difference is presented. Then the algorithm is described, and the effect of parameter variations

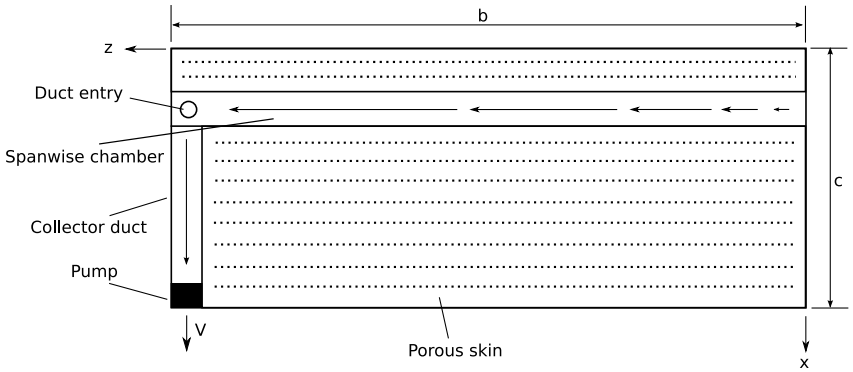

Fig. 11 Suction hardware layout, for an untapered wing of span b and chord c.

investigated. Finally, an approximate method for estimating the power associated with skin losses is given.

1. Pressure Drop Across a Porous Skin

The flow physics associated with sucking boundary-layer flow through a hole (or slot) has been well researched; here, in summarizing the main features, reference is made to the works by Gregory [6] and Thomas and Cornelius [29]. Essentially, there are two flow regimes: the external boundary-layer flow and the suction slot flow. For laminar flow applications, it is the flow immediately adjacent to the surface that is of importance in the first regime.

Gregory [6] stated that the flow in the hole, and hence the pressure drop across the surface, is a function of three dimensionless groups: the hole Reynolds number, aspect ratio (t_s/d), and Mach number. However, Thomas and Cornelius [29] and other researchers such as Doerrfer and Bohning [30] have pointed out that the pressure drop also depends on the crossflow velocity. Thomas and Cornelius thus added a fourth independent variable, characterizing the boundary-layer flow immediately adjacent to the surface by a nondimensional wall-velocity gradient.

Gregory [6] commented that, for very low flow rates, the pressure drop is roughly proportional to the velocity through the hole, corresponding to the viscous type flow region over which D'Arcy's law holds; for larger flow rates, inertial effects become more important, with the pressure drop becoming proportional to the square of the hole velocity until, for large Re_h, $\frac{\Delta P_s}{\frac{1}{2}\rho_w V_h^2} = fn(Re_h) \sim$ const. For LFC applications, Poll et al. [31] concluded that the flow through an individual hole is laminar, incompressible and pipe-flow-like, with the pressure drop having a quadratic dependence on the mass flow rate.

In spite of this body of work, no universal formula for the hole pressure drop has been agreed upon. Fortunately, for the present study, this obstacle can be circumvented as follows. On the basis of the existing literature, we assert that a hole diameter which corresponds to a high-Reynolds-number and low-Mach-number flow regime can always be found. Furthermore, the external crossflow at a given location is fixed, so now $\frac{\Delta P_s}{\frac{1}{2}\rho_w V_h^2} \sim$ const. This implies that the area-averaged suction velocity, in terms of the nondimensional pressure difference across the skin $\Delta\tilde{P}_s$, is given by

$$\frac{V_0}{U_\infty} = K_s \sqrt{\frac{\rho_\infty}{\rho_w} \Delta\tilde{P}_s} \tag{8}$$

where K_s depends on the chosen hole aspect ratio and the skin porosity. The former is constrained by our original assertion, but the latter remains under our control, and we therefore assume that the value of K_s can be set by the designer.

In principle, this would allow our optimized suction distribution to be realized for *any* chordwise $\Delta\tilde{P}_s$ distribution. In reality, the associated continual porosity variation would be impractical. Instead, we suggest that a single value of porosity, and hence K_s, would be associated with each chamber.

A final consideration is the flow temperature variation through an isolated hole in the porous surface. Doerrfer and Bohning [30] assume that the flow across a perforated plate is adiabatic. In contrast, Inger and Babinsky [32] prefer to take it to be isothermal, although they also note that the temperature change calculated from an adiabatic assumption would be small (because the flow Mach numbers on entry and exit are likely to be similar). Neither approach appears to have been directly substantiated; given our low-Mach-number constraint, both would give very similar results. However, the isothermal assumption would leave us unable to calculate the stagnation temperature at the hole exit. Therefore, in this paper, it is assumed that the flow is adiabatic. The stagnation temperature of the flow in the chamber is then equal to the static temperature on the external side of the skin.

2. Chamber Specification Algorithm

In the chordwise direction of a suction chamber, the pressure drop across the porous surface will change due to the surface pressure variation. As a result, the suction requirement to maintain laminar flow may no longer be satisfied [5]. An approximate analysis of this issue is presented in the Appendix; the result is repeated here:

$$\frac{(\frac{V_0}{U_\infty})_{\text{actual}}}{(\frac{V_0}{U_\infty})_{\text{required}}} \sim \sqrt{k - (-C_p)} \tag{9}$$

where k is a constant. Equation (9) reveals that, as $-C_p$ drops downstream of the suction peak, $(V_0/U_\infty)_{\text{actual}}$ increases at a faster rate than $(V_0/U_\infty)_{\text{required}}$; so choosing K_s to meet the suction requirement at the upstream edge of the chamber should ensure successful laminarization across its entire width. On the other hand, laminarization issues may arise with the increasing $-C_p$ upstream of the suction peak. We consider first the former, more usual, case.

Figure 12 shows a schematic of the internal and external pressures across a single chamber. The minimum and maximum pressure differences, $\Delta\tilde{P}_{s,\min}$ and $\Delta\tilde{P}_{s,\max}$, are design parameters which implicitly define the chamber width w_c. The required skin constant K_s is evaluated from Eq. (8), using $\Delta\tilde{P}_s(=\Delta\tilde{P}_{s,\min})$ and the optimal suction velocity $(V_0/U_\infty)_{\text{opt}}$ at the upstream end of the chamber. The

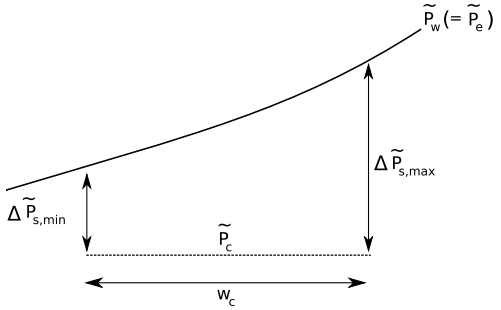

Fig. 12 Schematic of pressure variation over a single chamber width, downstream of the suction peak.

calculation proceeds downstream, calculating $(V_0/U_\infty)_{\text{actual}}$, continuously checking the laminar flow condition [since Eq. (9) is only an approximate guide], until $\Delta\tilde{P}_s > \Delta\tilde{P}_{s,\max}$. The optimal suction velocity at the start of the next chamber is then calculated on the basis of the current boundary-layer state.

For large $\Delta\tilde{P}_{s,\max}$, the boundary layer may be stabilized to such an extent that the required $(V_0/U_\infty)_{\text{opt}}$ at the start of the next chamber is negligible and, hence, the initial estimate of K_s too small to maintain laminar flow over that chamber. If this issue arises, K_s is increased iteratively until transition is avoided.

Upstream of the suction peak, the locations of $\Delta\tilde{P}_{s,\min}$ and $\Delta\tilde{P}_{s,\max}$ switch, as does Eq. (9)'s prediction for the most critical point. The skin constant is thus still set with $\Delta\tilde{P}_{s,\min}$, but using an optimum suction velocity calculated at the downstream end of the chamber. The actual suction distribution is then evaluated starting from the upstream end, as usual.

In summary, a chamber's pressure is set by specifying $\Delta\tilde{P}_{s,\min}$: $\tilde{P}_c = \tilde{P}_e - \Delta\tilde{P}_{s,\min}$; and its chordwise extent is determined by $\Delta\tilde{P}_{s,\max}$. Both of these parameters are constrained by the incompressible flow assumption implicit in the definition of the skin constant K_s. (The practical benefit of this constraint is an avoidance of possible choking problems that might otherwise arise.)

3. *Chamber Constraint Tradeoff Study*

To understand the influence of $\Delta\tilde{P}_{s,\min}$ and $\Delta\tilde{P}_{s,\max}$ on the suction power requirement, we introduce the parameters: $\Delta\tilde{P}_{s,\text{av}} = \frac{1}{2}(\Delta\tilde{P}_{s,\min} + \Delta\tilde{P}_{s,\max})$ and $\tilde{r}_c = \frac{\Delta\tilde{P}_{s,\max}}{\Delta\tilde{P}_{s,\min}}$. The first term characterizes the resistance of the porous surface, while the latter influences the sensitivity of the suction distribution over a chamber. The maximum value of each parameter is restricted by the incompressible flow assumption across the skin; a suitable range is $0.05 \le \Delta\tilde{P}_{s,\text{av}} \le 0.27$ and $2 \le \tilde{r}_c \le 4$. Figure 13 details the chordwise variation of $\Delta\tilde{P}_s$ corresponding to the upper limits specified, which give the greatest pressure difference; the critical pressure differential, corresponding to a hole Mach number of 0.4 ($P_c/P_{0,e} = 0.8703$), is superimposed.

Before we explore the suction requirements, consider Fig. 14, which shows the number of chambers as a function of $\Delta\tilde{P}_{s,\text{av}}$ and $\tilde{r}_c$. Here we see that, for a given $\tilde{r}_c$, the number reduces significantly initially, and then more gradually, with increasing $\Delta\tilde{P}_{s,\text{av}}$. This is due to the growing difference between $\Delta\tilde{P}_{s,\min}$ and $\Delta\tilde{P}_{s,\max}$. The rate of reduction decreases for higher values of $\tilde{r}_c$; however, increasing $\tilde{r}_c$ for a given $\Delta\tilde{P}_{s,\text{av}}$ results in fewer chambers.

The associated suction coefficient is plotted in Fig. 15. Here we see that C_Q is remarkably insensitive to $\Delta\tilde{P}_{s,\text{av}}$ and $\tilde{r}_c$. The former dependence is unsurprising, due to our use of varying skin resistance to meet suction targets. To understand the latter, consider Fig. 16,

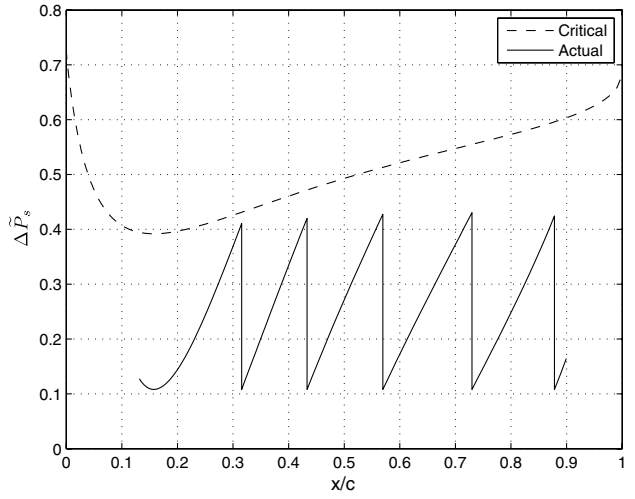

Fig. 13 Chordwise distribution of differential pressure across the porous skin with the critical pressure superimposed.

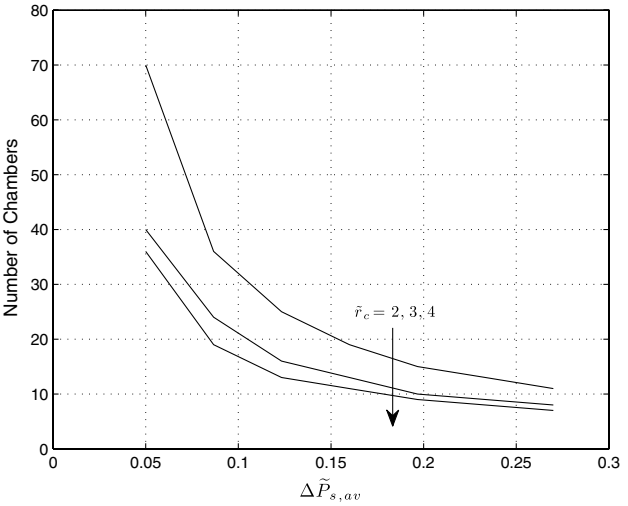

Fig. 14 Variation of the total number of chambers with $\Delta\tilde{P}_{s,\text{av}}$ and $\tilde{r}_c$.

which details the variation of the chordwise distribution of suction with $\Delta\tilde{P}_{s,\text{av}}$ and $\tilde{r}_c$, for the extremes considered above. Increasing $\tilde{r}_c$ increases the fluctuation of the suction distribution, but the average level of suction is insignificantly affected; oversuction towards the end of a chamber is almost exactly compensated by a reduced requirement at the start of the next. Figure 16 also confirms that increasing $\Delta\tilde{P}_{s,\text{av}}$ does not significantly affect the fluctuation, or overall magnitude, of the suction.

The corresponding $\tilde{W}_p$ variations are plotted in Fig. 17, showing that this parameter has a greater dependence on $\Delta\tilde{P}_{s,\text{av}}$ compared with $\tilde{r}_c$. This is unsurprising given the suction velocity behavior, which implies that the surface resistance correlates almost solely with $\Delta\tilde{P}_{s,\text{av}}$. The small increase in power with $\tilde{r}_c$ is attributed to the redistribution of suction, nearer the suction peak, where the stagnation pressure loss through the boundary layer is greatest. This effect is most prominent at higher values of $\Delta\tilde{P}_{s,\text{av}}$, as can be deduced from the chordwise distribution of suction detailed in Fig. 16.

The almost-linear dependence of $\tilde{W}_p$ on $\Delta\tilde{P}_{s,\text{av}}$ suggests that it may be possible to find a simple approximate relationship between the two. First, note that, due to our Mach-number constraint, the hole flow will be not far from incompressible. If we then additionally neglect variations in the pressure difference, we obtain

$$\tilde{W}_{p,s} \approx C_Q \Delta\tilde{P}_{s,\text{av}} \tag{10}$$

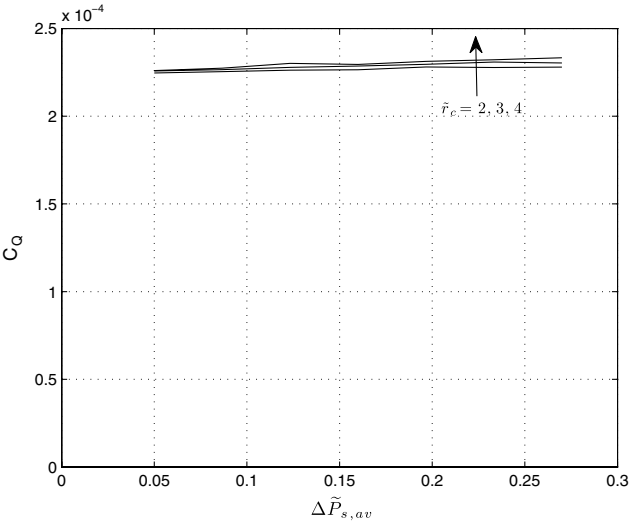

Fig. 15 Dependence of C_Q on $\Delta\tilde{P}_{s,\text{av}}$ and $\tilde{r}_c$. The optimal value calculated by the algorithm of Sec. II.B is $C_Q = 2.24 \times 10^{-4}$.

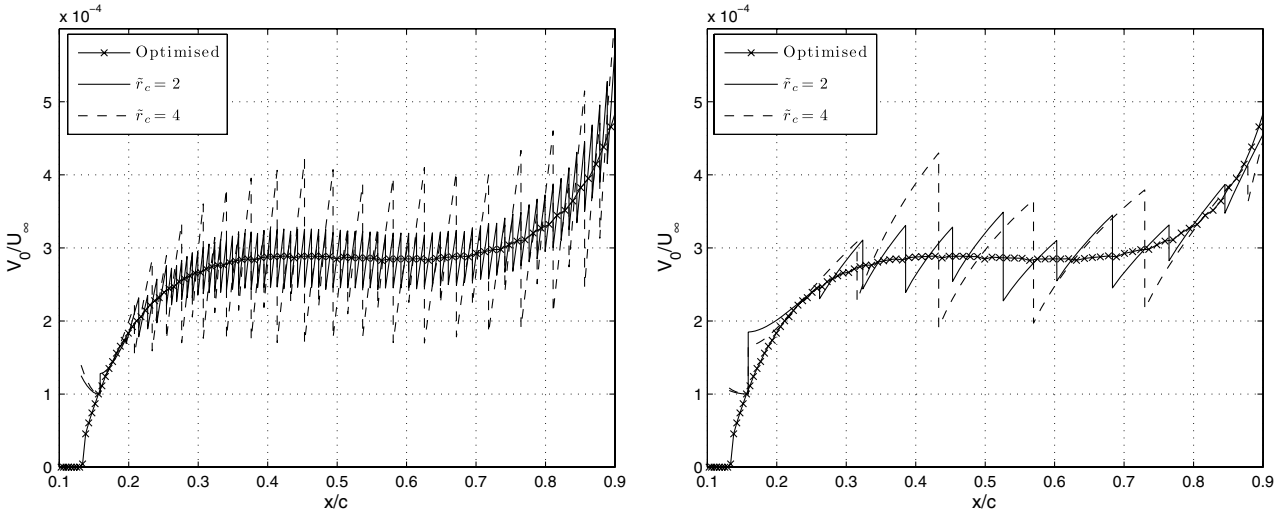

a) $\Delta\tilde{P}_{s,av}$ = 0.05 (for $\tilde{r}_c$ = 2 and 4, $C_Q = 2.25 \times 10^{-4}$ and 2.26×10^{-4}, respectively)

b) $\Delta\tilde{P}_{s,av}$ = 0.27 (for $\tilde{r}_c$ = 2 and 4, $C_Q = 2.28 \times 10^{-4}$ and 2.33×10^{-4}, respectively)

Fig. 16 Variation of chordwise distribution of suction with $\tilde{r}_c$ and $\Delta\tilde{P}_{s,\mathrm{av}}$.

for the power consumption associated with the skin. Finally, the minimal dependence of C_Q on the chamber design parameters means that it can be approximated by its optimal value. Adding the minimum power requirement associated with the optimized suction distribution to Eq. (10) gives an approximate estimate of the total power, which is also plotted in Fig. 17. There is excellent agreement between the two approaches; however, the incompressible flow assumption does begin to underestimate the power requirement somewhat at higher pressure differences, due to the differences between optimal and actual $C_Q s$, and the neglect of compressibility [accounted for in Eq. (6)].

Given the dependencies of the total number of chambers and power requirement, a reasonable choice of parameters might be $\Delta\tilde{P}_{s,\mathrm{av}} = 0.15$ and $\tilde{r}_c = 3$. The number of chambers is then 13, C_Q is 2.28×10^{-4} and $\tilde{W}_p$ is 3.70×10^{-4}. A breakdown of $\tilde{W}_p$ into the losses across the boundary layer and the skin is 3.32×10^{-4} and 0.38×10^{-4}, respectively; in comparison, the optimized suction distribution, with stagnation pressure loss through the boundary layer alone, has $\tilde{W}_p = 3.23 \times 10^{-4}$. Therefore, the redistribution of suction has had little adverse effect on the power requirement, and the increase due to the resistance of the porous skin is small, contributing only 10% to the total power.

C. Spanwise-Chamber Losses

With the chamber widths and baseline pressures now fixed, it is necessary to introduce the influence of spanwise-chamber losses. By discretizing the chamber in the spanwise direction, the pressure drop is calculated numerically. The sucked mass flow into the first element is known from the chamber pressure set to pass the flow across the porous skin. However, the chamber pressure then drops in the spanwise direction (due to inertial and wall-friction effects), the differential pressure across the skin increases and, consequently, so does the suction mass flow into the chamber. For each spanwise element, the pressure drop and suction rate are calculated iteratively. The converged chamber pressure is then used to begin the iteration

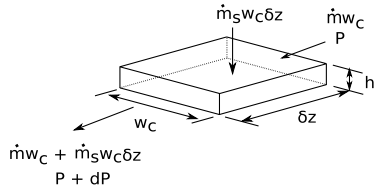

Fig. 18 Notation for chamber flow.

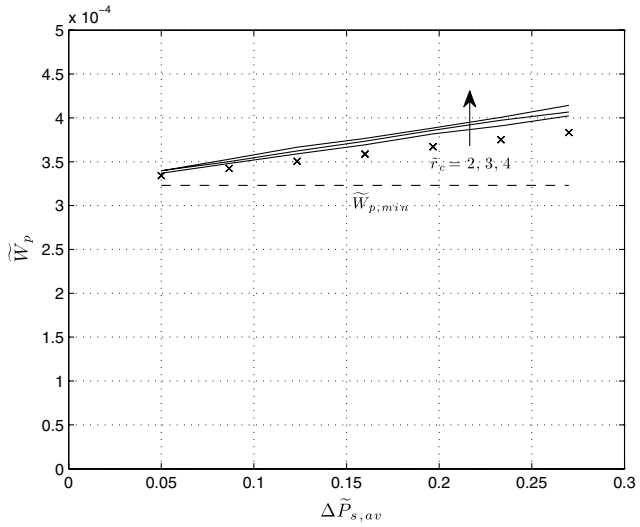

Fig. 17 Variation of actual (solid lines) and approximate (x markers) $\tilde{W}_p$ with $\Delta\tilde{P}_{s,\mathrm{av}}$ and $\tilde{r}_c$.

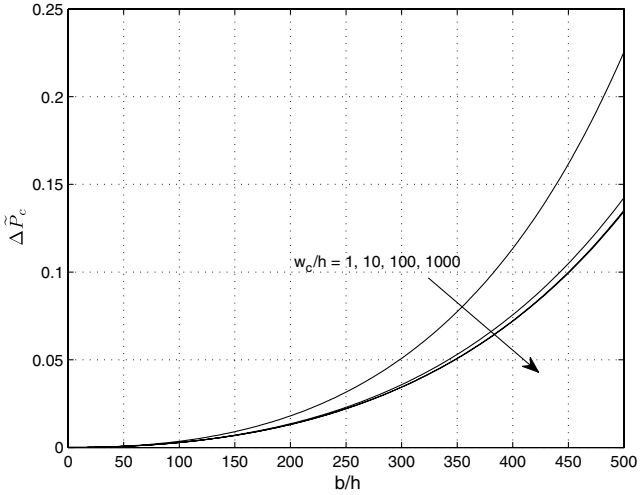

Fig. 19 Spanwise-chamber pressure drop dependence on b/h and w_c/h with $h = 10$ cm.

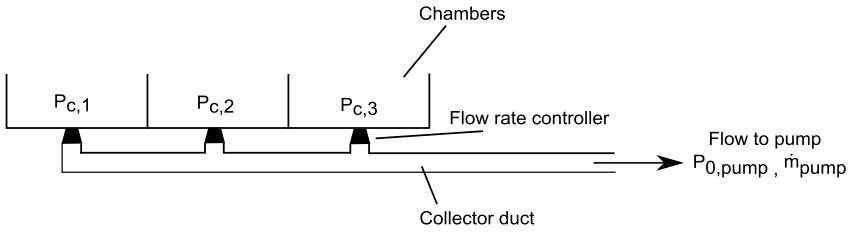

Fig. 20 Schematic of an alternative chamber-collector-duct arrangement.

over the next element. The laminar flow condition is also checked at each stage.

In analyzing the flow along a chamber, it is assumed that the chamber velocities are low enough to warrant the assumption of incompressible flow. By application of the 1-D momentum and mass continuity equations, and accounting for wall friction, the static pressure gradient over an element of length δz, width w_c, and height h, as illustrated in Fig. 18, is:

$$\frac{\mathrm{d}P}{\mathrm{d}z} = -\frac{2\dot{m}^2}{\rho_c h^2}\left(\frac{\dot{m}_s}{\dot{m}} + \frac{f}{D_{\mathrm{eq}}}\right) \tag{11}$$

The friction factor f is a function of $Re_{D_{\mathrm{eq}}}$ and D_{eq}: the latter influence is due to roughness effects. The equivalent diameter $D_{\mathrm{eq}} = 2h\frac{w_c/h}{1+w_c/h}$ must be used for rectangular conduits; and subsequently, $Re_{D_{\mathrm{eq}}} = \frac{2\dot{m}}{\mu}\frac{w_c/h}{1+w_c/h}$. The friction factor is calculated using the standard relation for laminar flow, while Churchill's correlation is used for turbulent flow; furthermore, the chambers are assumed to have the same roughness as drawn tubing [33].

The relevant geometrical parameters affecting the pressure drop over a span b are b/h and w_c/h (through D_{eq}). To understand the influence of these parameters, we investigate the pressure loss along a single spanwise chamber with external flow properties equivalent to those at an altitude of 10,900 m and $M_\infty = 0.56$, and having: a constant external chordwise suction distribution of $V_0/U_\infty = 3.29 \times 10^{-4}$; a skin porosity $K_s = 11.0 \times 10^{-4}$; and typical surface and chamber pressures of $\tilde{P}_e = 4.58$ and $\tilde{P}_c = 4.49$, respectively.

Figure 19 details the variation of $\Delta\tilde{P}_c$ with b/h and w_c/h, for a constant chamber depth h of 10 cm. As expected, there is a strong dependence on b/h. Initially, $\Delta\tilde{P}_c$ decreases with w_c/h, and then becomes independent of this parameter for higher values. Plots for other values of h are very similar, but not identical, due to Reynolds number dependence.

To interpret these results, it is helpful to assume that the pressure drop is small enough to warrant the approximation $\dot{m}_s \approx$ constant; and that the friction factor is constant along the length of a chamber. Then, on integration of Eq. (11), the nondimensional chamber pressure drop becomes:

$$\Delta\tilde{P}_c = -\frac{2\dot{m}_s^2}{\rho_c \rho_\infty U_\infty^2}\left(\frac{b}{h}\right)^2\left[1 + \frac{f}{3}\left(\frac{b}{h}\right)\left(\frac{1+w_c/h}{w_c/h}\right)\right] \tag{12}$$

This suggests that we could expect the inertial term's contribution to the pressure drop to be approximately quadratic in b/h, and the friction term's to be cubic. The explicit dependence on w/h is restricted to the friction term, and disappears for wide, shallow chambers. These observations are consistent with the results of Fig. 19.

From the design viewpoint, Eq. (12) shows that the spanwise extent of chambers must be limited to avoid excessive losses. If the friction contribution is not to exceed the inertial, and we take $f \simeq 0.01$, then we require $b/h \lesssim 300$ (for shallow chambers). At a typical value of $\dot{m}_s^2$, we have $\dot{m}_s^2/\rho_w\rho_\infty U_\infty^2 \simeq 10^{-7}$, giving $\Delta\tilde{P}_c \simeq 0.036$ at the upper limit. Thus, for example, 10-cm-deep chambers could run for 30 m with negligible pressure drop, suggesting that the power losses from this source should be avoidable in a practical design.

D. Collector Duct Tradeoff Study

We assume that the collector ducts are large enough for skin-friction losses to be negligible. The power calculations in Sec. V.B then correspond to a system architecture having one collector duct and pump per chamber. This, however, is likely to become impractical for a large number of chambers. An alternative arrangement where the flow from multiple chambers is collected by a single collector duct is detailed schematically in Fig. 20. As the required static pressures of adjacent chambers ($P_{c,1}$, $P_{c,2}$, $P_{c,3}$, etc.) differ, flow rate control devices (e.g., orifice plates) are then needed. The collector duct stagnation pressure $P_{0,d}$ is set by the lowest static pressure among the chambers which feed it.

Here we aim to understand the tradeoff between the power requirement and the number of chambers and collector ducts. The final number of ducts (and pumps) must be based on a consideration of geometric constraints and power requirements. More ducts imply increased complexity, but lower average pressure loss from chamber to pump.

The pressure losses associated with throttling the flows from the chambers can be minimized by having an approximately equal number of chambers per collector. If the total chamber number is not an integer multiple of the collector number, the first residual chamber is added to the last collector arrangement, and the remainder allocated to successive arrangements starting from the first. Figure 21 provides an example illustration of the pressure distribution corresponding to 13 chambers and four collectors: each collector has a minimum of three chambers, with the last having four.

The variation of $\tilde{W}_p$ with the total number of collector ducts, for different $\tilde{r}_c s$, is detailed in Fig. 22. Consider the case where $\tilde{r}_c = 2$ (which gives 19 chambers) first: one collector duct, having a pressure offset from the suction peak pressure of $\Delta\tilde{P}_{s,\mathrm{av}}(=0.15)$, gives the greatest power requirement, but $\tilde{W}_p$ starts to asymptote very quickly; by five collectors the power penalty is only 10%. As $\tilde{r}_c$ is increased, the number of chambers, and hence the maximum number of collector ducts decreases; interestingly, this insignificantly affects the power variation and its magnitude: for a given number of collector ducts and average skin pressure drop, there are no direct benefits to be

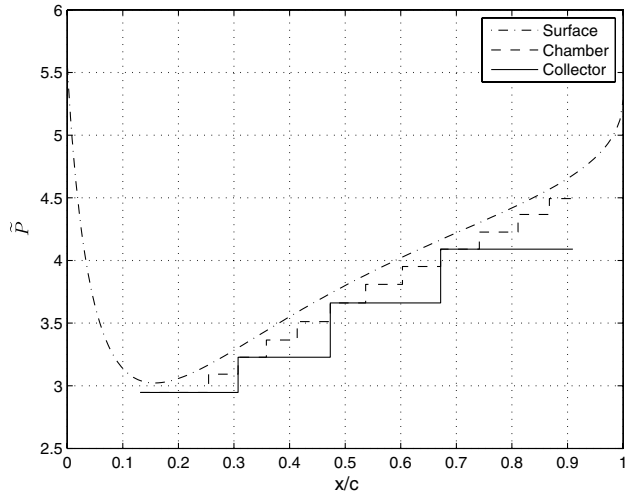

Fig. 21 Comparison of surface, chamber and collector static pressures: $\Delta\tilde{P}_{s,\mathrm{av}} = 0.15$ and $\tilde{r}_c = 3$.

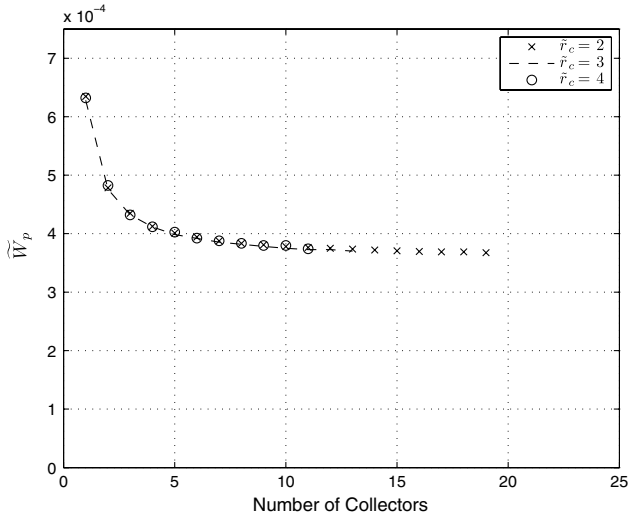

Fig. 22 Variation of $\tilde{W}_p$ with the number collectors and $\tilde{r}_c$, with $\Delta\tilde{P}_{s,\mathrm{av}} = 0.15$.

had from increasing the number of chambers and trying to maintain a near-optimal suction distribution. (There may, nonetheless, be indirect benefits, specifically if the chamber sidewalls also have a role as structural stiffeners.) This observation, should, in fact, be no great surprise; the overall average pressure drop between the suction surface and the pumps is now set by the number of collector ducts, and the only potential benefit in having more chambers is to ensure a suction distribution closer to optimal. However, as we have seen, departures from the optimum have very little effect on overall suction volumes, and hence also on power consumption.

VI. Conclusions

Eppler and Somers' [12] semi-empirical boundary-layer stability algorithm has been implemented to determine the optimal distribution of suction required to maintain laminar flow over a desired region, for a specified aerofoil geometry, surface pressure distribution, and chord Reynolds number. To facilitate the design of a practical suction system, an automated algorithm has been developed, requiring only the specification of the porous skin's surface resistance and the sensitivity of the suction distribution (represented by an average pressure drop across the skin $\Delta\tilde{P}_{s,\mathrm{av}}$ and the maximum-to-minimum pressure difference ratio $\tilde{r}_c$ across a chamber), to define a set of subsurface chamber widths and pressures. The method assumes that, for a given chamber pressure distribution, the corresponding real suction distribution and power calculation can be found without needing to calculate suction hole velocities explicitly; however, the pressure difference across the skin should be such that flow remains subsonic (and incompressible). The spanwise-chamber pressure drop required to overcome frictional and inertial effects has been investigated, and, finally, the effects of collector ducts (introduced to reduce system architecture complexity) on the power requirement have been explored.

The study identified a minimum power requirement independent of the suction system design; this is associated with the boundary-layer stagnation-pressure loss of the flow in an optimal suction distribution (one which maintains a neutrally stable laminar boundary layer). Deviations from the optimal suction distribution, due to a practical porous-skin and suction-chamber architecture, have very little effect on the overall suction coefficient, but additional power is required, due to the skin resistance. To a good approximation, this power penalty is given by the product of the optimal suction flow rate coefficient and the average skin pressure drop. In the spanwise direction, the effect of the chamber pressure drop due to frictional and inertial effects is two-fold: first, it gives rise to excess suction, and second, it combines with the excess suction to increase the pressure losses. However, in practice, through suitable choice of spanwise length-to-chamber depth, it should be possible to make this contribution to the overall power requirement negligible. Finally, if there are fewer collector ducts (and hence pumps) than chambers, it is the average pressure drop from the aerofoil surface to the collector ducts, rather than to the chambers, that determines the power penalty.

With regard to the conceptual design of an LFW, it has been confirmed that a suction system consuming little more power than the optimum value is a practical possibility. However, a representative aerofoil pressure distribution and associated suction profile are necessary to obtain an accurate estimate of this optimum. Once these are available, the system architecture may be specified by the following algorithm:

1) Set the average skin pressure drop, $\Delta\tilde{P}_{s,\mathrm{av}}$.
2) Decide the number of suction pumps.
3) Choose the pressure ratio parameter $\tilde{r}_c$ so that the number of chambers is equal to the number of pumps.
4) Check suction hole Mach numbers and, if too high, iterate from [2].
5) Estimate skin resistance power penalty and, if necessary (either the penalty or the number of pumps is too high) iterate from [1].
6) Set the chamber depth so that spanwise pressure losses are negligible [c.f. Eq. (12)].

On the basis of the typical LFW design parameters used in this study, such an approach can be expected to produce a design consuming at most 20%, and more likely around 10%, excess power over the optimum value.

Appendix

The analysis presented here aims to determine a relationship between the suction required for laminarization and that which can actually be achieved for a specified porous surface, as a function of the aerofoil's surface pressure distribution. First, the former is considered.

Eliminating u_e'/u_e from the boundary-layer integral Eqs. (1) and (2), and assuming suction maintains the boundary layer on the verge of transition such that $\delta_2' = \delta_3' = 0$, we obtain:

$$(2 + H_{12})\frac{\delta_2}{3\delta_3}\left(C_d - \frac{V_0}{u_e}\right) = C_f - \frac{V_0}{u_e} \tag{A1}$$

Under our assumptions, the shape factor H_{32} is constant, so both C_f and C_d vary only with the external (potential) flow velocity ratio u_e/U_∞, as $(u_e/U_\infty)^{-1}$. For incompressible flow the velocity ratio is related to C_p by:

$$\frac{u_e}{U_\infty} = \sqrt{1 - C_p} \tag{A2}$$

Hence the scaling for the required V_0/u_e is:

$$\left(\frac{V_0}{u_e}\right)_{\mathrm{required}} \sim \frac{1}{\sqrt{1 - C_p}} \tag{A3}$$

For our practical, chamber-based implementation, the skin pressure drop is:

$$\Delta\tilde{P}_s = C_p + \tilde{P}_\infty - \tilde{P}_c \tag{A4}$$

Combining this with Eq. (8), we see how V_0 varies with C_p:

$$\left(\frac{V_0}{u_e}\right)_{\mathrm{actual}} \sim \sqrt{\frac{k + C_p}{1 - C_p}} \tag{A5}$$

where $k = \tilde{P}_\infty - \tilde{P}_c$ is a constant.

Combining Eqs. (A3) and (A5):

$$\frac{(\frac{V_0}{U_\infty})_{\mathrm{actual}}}{(\frac{V_0}{U_\infty})_{\mathrm{required}}} \sim \sqrt{k - (-C_p)} \tag{A6}$$

Acknowledgments

The authors thank H. Babinsky from the University of Cambridge for the useful discussions on the pressure drop across a porous skin, and his general advice. The authors acknowledge the implementation of the Ladson and Brooks Computational Program by W. H. Mason of the Virginia Polytechnic Institute and State University. The first author thanks the UK Engineering and Physical Sciences Research Council for its financial support via its Doctoral Training scheme.

References

[1] Green, J. E., "Greener by Design: The Technology Challenge," *The Aeronautical Journal*, Vol. 106, No. 1056, 2002, pp. 57–113.

[2] Hall, P., Malik, M. R., and Poll, D. I. A., "On the Stability of an Infinite Swept Attachment Line Boundary Layer," *Proceedings of the Royal Society of London, Series A: Mathematical and Physical Sciences*, Vol. 395, No. 1809, 1984, pp. 229–245.

[3] Green, J. E., "Laminar Flow Control: Back to the Future," *38th Fluid Dynamics Conference and Exhibit*," AIAA Paper 2008-3738, 2008.

[4] Pfenninger, W., "Laminar Flow Control, Laminarization: Special Course on Drag Reduction," AGARD R-654, 1977.

[5] Lachmann, G. V., "Boundary Layer Control," *The Journal of the Royal Aeronautical Society*, Vol. 59, No. 531, 1955, pp. 163–198.

[6] Gregory, N., *Research on Suction Surfaces for Laminar Flow, Boundary Layer and Flow Control*, edited by G. V. Lachmann, Vol. 2, Pergamon Press, Oxford, England, U.K., 1961, pp. 924–960.

[7] Head, M. R., "The Boundary Layer with Distributed Suction," Aeronautical Research Council Tech. Rept. No. 2783, 1955.

[8] Pearce, W. E., "Evaluation of Laminar Flow Control System Concepts for Subsonic Commercial Transport Aircraft," NASA CR-159251, 1983.

[9] Saeed, T. I., Graham, W. R., Babinsky, H., Eastwood, J. P., Hall, C., Lone, M. M., Jarrett, J. P., and Seffen, K. A., "Conceptual Design for a Laminar Flying Wing Aircraft," AIAA Paper 2009-3616, 2009.

[10] Head, M. R., "Approximate Calculations of the Laminar Boundary Layer with Suction, with Particular Reference to the Suction Requirements for Boundary Layer Stability on Aerofoils of Different Thickness/Chord Ratios," Aeronautical Research Council Tech. Rept. No. 3124, 1959.

[11] Joslin, R. D., "Aircraft Laminar Flow Control," *Annual Review of Fluid Mechanics*, Vol. 30, 1998, pp. 1–29. doi:10.1146/annurev.fluid.30.1.1

[12] Eppler, R., and Somers, D. M., "A Computer Program for the Design and Analysis of Low-Speed Airfoils," NASA TM-80210, 1980.

[13] Bowers, A. H., and Sim, A. G., "A Comparison of Wortmann Airfoil Computer-Generated Lift and Drag Polars with Flight and Wind Tunnel Results," NASA TM-86035, 1984.

[14] Drela, M., and Giles, M. B., "Viscous-Inviscid Analysis of Transonic and Low Reynolds Number Airfoils," *AIAA Journal*, Vol. 25, No. 10, 1987, pp. 1347–1355. doi:10.2514/3.9789

[15] Ellis, J. E., Walsh, S. A., and Poll, D. I. A., "Assessment of the e^N Method as a Transition Prediction Tool for Zero Pressure Gradient Flows with and Without Boundary Layer Suction," *Aerodynamic Drag Reduction Technologies, Notes on Numerical Fluid Mechanics*, edited by P. Thiede, Vol. 76, Springer, New York, 2000.

[16] Eppler, R., "Turbulent Airfoils for General Aviation," *Journal of Aircraft*, Vol. 15, No. 2, 1978, pp. 93–99. doi:10.2514/3.58320

[17] Berry, S. A., "Incompressible Boundary-Layer Stability Analysis of LFC Exp. Data for Sub-Critical Mach Numbers," NASA CR-3999, 1989.

[18] Viken, J., and Wagner, R. D., "Design Limits of Compressible NLF Airfoils," AIAA Paper 91-0067, 1991.

[19] Mack, L. M., "On the Stability of the Boundary Layer on a Transonic Swept Wing," AIAA Paper 79-0264, 1979.

[20] Harris, C. D., Harvey, W. D., and Brooks, C. W., Jr., "The NASA Langley Laminar-Flow-Control Experiment on a Swept, Supercritical Airfoil," NASA TP-2809, 1988.

[21] Atkin, C., "Performance Tradeoff Studies for a Retrofit Hybrid Laminar Flow Control System," AIAA Paper 2004-2215, 2004.

[22] Bushnell, D. M., and Malik, M. R., "Supersonic Laminar Flow Control," NASA 90N-12554, 1987.

[23] Berry, S. A., Dagenhart, J., Brooks, C. W., Jr., and Harris, C. D., "Boundary Layer Stability Analysis of LaRC 8-foot LFC Experimental Data," NASA 90N-12532, 1987.

[24] Young, A. D., *Boundary Layers*, AIAA Education Series, AIAA, Washington, D.C., 1989.

[25] Ladson, C. L., and Brooks, C. W., Jr., "Development of a Computer Program to Obtain Ordinates for NACA 6- and 6A-Series Airfoils," NASA TM X-3069 1974.

[26] Rioual, J. L., Nalson, P. A., Hackenberg, P., and Tutty, O. R., "Optimum Drag Balance for Boundary-Layer Suction," *Journal of Aircraft*, Vol. 33, No. 2, 1996, pp. 435–438.

[27] Edwards, J. B., "Fundamental Aspects of Propulsion for Laminar Flow Aircraft, Boundary Layer and Flow Control," edited by G. V. Lachmann, Vol. 2, Pergamon Press, Oxford, England, U.K., 1961, pp. 1077–1122.

[28] Pankhurst, R. C., and Gregory, N., "Power Requirements for Distributed Suction for Increasing Maximum Lift," Aeronautical Research Council Tech. Rept. C.P. No. 82, 1952.

[29] Thomas, A. S. W., and Cornelius, K. C., "Investigation of a Laminar Boundary-Layer Suction Slot," *AIAA Journal*, Vol. 20, No. 6, 1982, pp. 790–796. doi:10.2514/3.51136

[30] Doerffer, P. P., and Bohning, R., "Modelling of Perforated Plate Aerodynamics Performance," *Aerospace Science and Technology*, Vol. 4, No. 8, 2000, pp. 525–534. doi:10.1016/S1270-9638(00)01063-4

[31] Poll, D. I. A., Danks, M., and Humphreys, B. E., "The Aerodynamic Performance of Laser Drilled Sheets," *1st European Forum on Laminar Flow Technology*, Hamburg, Germany, 1992, pp. 274–277.

[32] Inger, G. R., and Babinsky, H., "Viscous Compressible Flow Across a Hole in a Flat Plate," *Journal of Aircraft*, Vol. 37, No. 6, 2002, pp. 1028–1032. doi:10.2514/2.2707

[33] Menon, E. S., *Piping Calculations Manual*, McGraw–Hill, New York, 2004.